even in the dc limit so that a large number of cells may be required to determine the average SAR. Since limits which have been specified for the electrical size ($kL$) of a cell with block models pertain only to FDE [20], such conditions are necessary but not sufficient for convergence.

In calculations made for objects having corners and edges, the volume-average SAR may converge more slowly than values of local SAR at locations distant from the corners and edges. An extrapolant may be used to make substantial corrections for FIE in order to estimate the average SAR with such objects. Extrapolation fails when there is appreciable FDE since the procedure requires that the individual samples of local SAR do not have appreciable error. Interpolants have also been used to make corrections to values of average SAR; but the extrapolant makes a substantially larger correction, so it is the procedure of choice when solutions are available having two or more discretizations. Only values of average SAR obtained without interpolation should be used with the extrapolant since such values have errors which vary linearly with cell size.

We consider it to be essential that the array of cubes used for a block model be arranged for a best-fit of the object to be modeled. Since the electric field has sizable variation near corners and edges, it is necessary that such shapes not be emphasized when modeling a smooth object such as the human body. Increasing the number of cells in a model by subdividing one or more of the cells and retaining the same outer boundary is one way of creating such an emphasis. It appears that when others have used such simple subdivisions with block models of man their results departed from solutions for man and instead approached solutions for models having unwanted corners and edges [9]–[11].

It is anticipated that block model solutions for objects having smooth shapes, such as models of man, will have considerably less FIE than occurs with the dielectric cube so that convergence will be more rapid than is seen in the present examples. In yet-unpublished work, we have found that the values of volume-average SAR for block models of a man-sized prolate spheroid at 100 and 225 MHz are within 6 percent of those calculated for the prolate spheroid by other methods. Comparisons of the local values of SAR in both prolate spheroids and spheres with block model solutions for those objects are in progress.

## References


[1] M. J. Hagmann, O. P. Gandhi, and C. H. Durney, "Numerical calculation of electromagnetic energy deposition for a realistic model of man," *IEEE Trans. Microwave Theory Tech.*, vol. MTT-27, pp. 804–809, Sept. 1979.

[2] D. E. Livesay and K. M. Chen, "Electromagnetic fields induced inside arbitrarily shaped biological bodies," *IEEE Trans. Microwave Theory Tech.*, vol. MTT-22, pp. 1273–1280, Dec. 1974.

[3] G. W. Hohmann, "Three-dimensional induced polarization and electromagnetic modeling," *Geophysics*, vol. 40, pp. 309–324, Apr. 1975.

[4] M. J. Hagmann, O. P. Gandhi, J. A. D'Andrea, and I. Chatterjee, "Head resonance: Numerical solutions and experimental results," *IEEE Trans. Microwave Theory Tech.*, vol. MTT-27, pp. 809–813, Sept. 1979.

[5] M. J. Hagmann and O. P. Gandhi, "Numerical calculation of electromagnetic energy deposition in man with ground and reflector effects," *Radio Sci.*, vol. 14, pp. 23–29, Nov.–Dec. 1979.

[6] O. P. Gandhi, M. J. Hagmann, and J. A. D'Andrea, "Part-body and multibody effects on absorption of radio frequency electromagnetic energy by animals and by models of man," *Radio Sci.*, vol. 14, pp. 15–21, Nov.–Dec. 1979.

[7] G. M. Hahn, "Hyperthermia for the engineer: A short biological primer," *IEEE Trans. Bio-Med. Eng.*, vol. BME-31, pp. 3–8, Jan. 1984.

[8] R. F. Harrington, *Field Computation by Moment Methods*. New York: Macmillan, 1968.

[9] J. F. Deford, O. P. Gandhi, and M. J. Hagmann, "Moment-method solutions and SAR calculations for inhomogeneous models of man with large number of cells," *IEEE Trans. Microwave Theory Tech.*, vol. MTT-31, pp. 848–851, Oct. 1983.

[10] E. H. Wissler, "Final report: Thermal and nonthermal effects of microwave radiation," Dept. Chemical Eng., University of Texas at Austin, National Institutes of Health grant GM27844, Mar. 1983.

[11] H. Massoudi, C. H. Durney, and M. F. Iskander, "Limitations of the cubical block model of man in calculating SAR distributions," *IEEE Trans. Microwave Theory Tech.*, vol. MTT-32, pp. 746–752, Aug. 1984.

[12] S. W. Lee, J. Boersma, C. L. Law, and G. A. Deschamps, "Singularity in Green's function and its numerical evaluation," *IEEE Trans. Antennas Propagat.*, vol. AP-28, pp. 311–317, May 1980.

[13] A. Stogryn, "Equations for calculating the dielectric constant of saline water," *IEEE Trans. Microwave Theory Tech.*, vol. MTT-19, pp. 733–736, Aug. 1971.

[14] B. S. Guru and K. M. Chen, "Experimental and theoretical studies on electromagnetic fields induced inside finite biological bodies," *IEEE Trans. Microwave Theory Tech.*, vol. MTT-24, pp. 433–440, July 1976.

[15] K. M. Chen and B. S. Guru, "Internal EM field and absorbed power density in human torsos induced by 1–500-MHz EM waves," *IEEE Trans. Microwave Theory Tech.*, vol. MTT-25, pp. 746–756, Sept. 1977.

[16] M. J. Hagmann, "Numerical studies of absorption of electromagnetic energy by man," Ph.D. dissertation, Dept. Elec. Eng., Univ. Utah, Salt Lake City, UT, Dec. 1978.

[17] E. M. Purcell and C. R. Pennypacker, "Scattering and absorption of light by nonspherical dielectric grains," *Astrophys. J.*, vol. 186, pp. 705–714, Dec. 1973.

[18] R. Mittra and C. A. Klein, "Stability and convergence of moment-method solutions," in *Numerical and Asymptotic Techniques in Electromagnetics*, R. Mittra, Ed. New York: Springer-Verlag, 1975, ch. 5.

[19] M. J. Hagmann, O. P. Gandhi, and C. H. Durney, "Improvement of convergence in moment-method solutions by the use of interpolants," *IEEE Trans. Microwave Theory Tech.*, vol. MTT-26, pp. 904–908, Nov. 1978.

[20] M. J. Hagmann, O. P. Gandhi, and C. H. Durney, "Upper bound on cell size for moment-method solutions," *IEEE Trans. Microwave Theory Tech.*, vol. MTT-25, pp. 831–832, Oct. 1977.


# *E*-Plane Integrated Parallel-Strip Screen Waveguide Filters

FRITZ ARNDT, SENIOR MEMBER, IEEE, JOHANNES BEIKE, DIETRICH GRAUERHOLZ, CHRISTOPH LINGEMANN, AND JENS BORNEMANN

***Abstract*—A rigorous field theory design of a class of rectangular waveguide screen filters is presented which achieves improved attenuation in the upper stopband. The method of field expansion into suitable eigenmodes used considers the effects of the finite rectangular *E*-plane grid thickness and the mutual higher order mode interaction of the single screens. Calculated results up to 55 GHz show that the peak attenuation in the upper stopband for a *Ka*-band (26–40-GHz) two-resonators filter example with a midband frequency of $f_0 = 37$ GHz is about 70 dB, whereas its planar circuit single-metal-insert counterpart reaches only about 34 dB. A *Ku*-band (12–18-GHz) filter prototype with three metal-etched screens yields a measured passband insertion loss of 0.8 dB at about $f_0 = 17$ GHz and a measured attenuation in upper stopband of about 50 dB up to 25 GHz.**

## I. Introduction

Metal inserts placed in the *E*-plane of rectangular waveguides achieve low-cost low-loss filter designs [1], [2]. Especially for filters with midband frequencies in the near of the higher band end of the corresponding waveguide housing, the attenuation in the upper stopband attainable with single inserts, however, is often too low [3] for many applications. This is due to unwanted

Manuscript received November 28, 1983; revised February 25, 1985.

The authors are with the Microwave Department, University of Bremen, Kufsteiner Strasse, NW 1, D-2800 Bremen 33, West Germany.

0018-9480/85/0700-0654$01.00 ©1985 IEEE

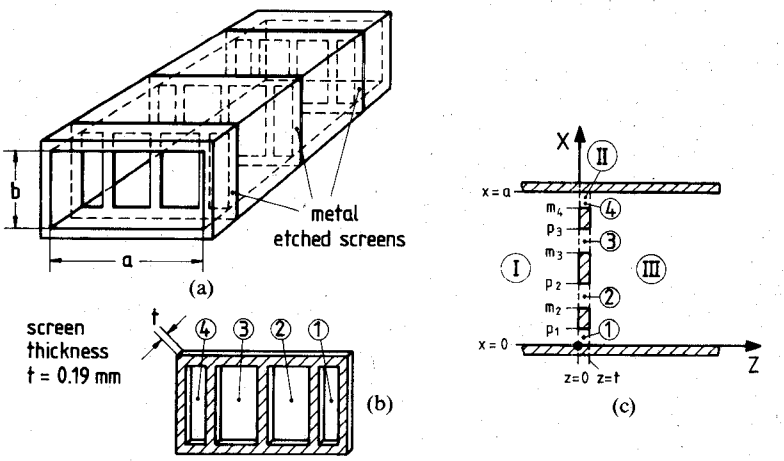


Fig. 1. *E*-plane waveguide screen filter. (a) Waveguide and screens. (b) Subregions for the field theory treatment.

coupling of the higher order modes generated by a single inductive post [4], [5] as a reactance element. To reduce this effect, triple-strip screens (Fig. 1) can be used.

The advantages of a triplet of round posts in suppressing higher order modes up to the sixth order have already been pointed out in [4]–[9]. In comparison with the round post configuration, however, the strip structure of Fig. 1 has the advantage of being producible by the metal-etching technique, which is appropriate for low-cost mass production and avoids the necessity for tuning devices for the filter. Moreover, it may be stated that broadside strips in the rectangular waveguide may achieve still slightly higher peak attenuation in the upper stopband than round posts of identical susceptance considering related investigations at equivalent quadratic post structures.

Inductive strips have already been analyzed using variational methods [10], [11] and the moment method [9]. However, the immediate higher order mode interaction between series-connected strip elements, which influences considerably the stopband behavior of related filter structures, is not taken into account by these lumped-element network descriptions. Also, the effect of the finite thickness of the strips altering passband ripple behavior and midband frequency has been hitherto neglected.

In this paper, therefore, similar to the *E*-plane filter calculation in [2], the design of optimized screen filters (Fig. 1) is based on a rigorous field expansion into suitable incident and scattered waves at all discontinuities, beyond as well as below the cutoff frequencies. This allows direct inclusion of both higher order mode coupling and finite strip thickness. Matching the fields at the discontinuity interfaces yields the corresponding scattering matrices, which are directly combined with the intermediate waveguide sections to the overall scattering matrix of the filter. A simple optimization computer program varies the screen dimensions until the insertion loss within the passband yields a minimum and the stopband attenuation an optimum. The evolution strategy method [12] is applied where no differentiation step in the optimization process is necessary.

## II. Theory

Like the metal insert filter [2], the design of rectangular screen filters is based on field expansion into orthogonal eigenmodes in the subregions together with field matching at common interfaces. For each subregion $\nu = \mathrm{I}, \mathrm{II1}, \mathrm{II2}, \mathrm{II3}, \mathrm{II4}$ (Fig. 1(b)), the fields at the discontinuity $z = 0$

$$\vec{E}^{(\nu)} = -j\omega\mu\nabla \times \vec{\Pi}_{hx}^{(\nu)} \quad \vec{H}^{(\nu)} = \nabla \times \nabla \times \vec{\Pi}_{hx}^{(\nu)} \tag{1}$$

are derived from the $x$-component of the magnetic Hertzian vector $\vec{\Pi}_h$, which is assumed to be the sum of suitable eigenmodes satisfying the wave equation and the boundary conditions at the metallic surfaces at $x = 0, p_1, m_2, p_2, m_3, p_3, m_4, a$

$$\Pi_{hx}^{(\nu)} = \sum_{m=1}^{\infty} A_m^{(\nu)\pm} T_m^{(\nu)} \cdot \sin\left[\frac{m\pi}{p^{(\nu)}} \cdot f^{(\nu)}\right] \cdot e^{\mp jk_{zm}^{(\nu)} \cdot z} \tag{2}$$

with

$$\left(f^{(\nu)}\right)' = (x, x, p_2 - x, p_3 - x, a - x)$$

$$\left(p^{(\nu)}\right)' = (a, p_1, p_2 - m_2, p_3 - m_3, a - m_4)$$

$$k_{zm}^{(\nu)2} = k^2 - \left(\frac{m\pi}{p^{(\nu)}}\right)^2, \qquad k^2 = \omega^2\mu\epsilon \tag{3}$$

and

$$T_m^{(\nu)} = \frac{1}{k_{zm}^{(\nu)}\sqrt{\omega\mu k_{zm}^{(\nu)}}} \cdot \begin{cases} \sqrt{\dfrac{2}{ba}}, & \nu = \mathrm{I} \\ \sqrt{\dfrac{2}{bp_1}}, & \nu = \mathrm{II1} \\ \sqrt{\dfrac{2}{b(p_2 - m_2)}}, & \nu = \mathrm{II2} \\ \sqrt{\dfrac{2}{b(p_3 - m_3)}}, & \nu = \mathrm{II3} \\ \sqrt{\dfrac{2}{b(a - m_4)}}, & \nu = \mathrm{II4} \end{cases} \tag{4}$$

$A_m^{(\nu)\pm}$ are the still unknown eigenmode amplitude coefficients of the forward and backward waves, which are suitably normalized by $T_m$ so that the power carried by a given wave is $1W$ for a wave amplitude coefficient of $\sqrt{1W}$.

By matching the tangential field components at the common interfaces at the step discontinuities at $z = 0$ (Fig. 2(a)), the coefficients $A_m^{(\nu)\pm}$ can be related to each other after multiplication with the appropriate orthogonal function

$$\vec{A}^{\mathrm{I}+} + \vec{A}^{\mathrm{I}-} = \sum_{\eta=1}^{4} \left(L^{(\eta)}\right) \cdot \left[\vec{A}^{\mathrm{II}(\eta)+} + \vec{A}^{\mathrm{II}(\eta)-}\right]$$

$$\left(N^{(\eta)}\right) \cdot \left[\vec{A}^{\mathrm{I}+} - \vec{A}^{\mathrm{I}-}\right] = \vec{A}^{\mathrm{II}(\eta)+} - \vec{A}^{\mathrm{II}(\eta)-},$$

$$\eta = 1,2,3,4 \qquad \text{(cf. Fig. 2(a))}. \tag{5}$$

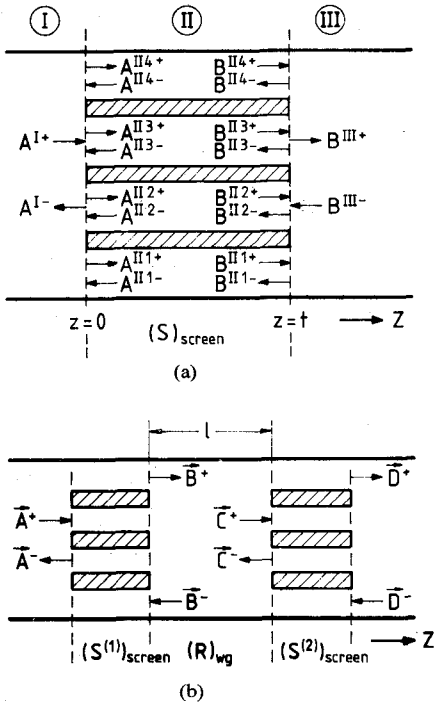


Fig. 2. Forward (+) and backward (−) waves (a) at the discontinuities at $z = 0$ and $z = t$ and (b) at two series connected screens.

The abbreviations $(L^{(\eta)})$ and $(N^{(\eta)})$ are elucidated in the Appendix. Similar to [2], (5) yields the scattering matrix for the set of discontinuities at $z = 0$ (Fig. 2(a))

$$\begin{pmatrix} \vec{A}^{I-} \\ \vec{A}^{III+} \\ \vec{A}^{II2+} \\ \vec{A}^{II3+} \\ \vec{A}^{II4+} \end{pmatrix} = (S)_{z=0} \begin{pmatrix} \vec{A}^{I+} \\ \vec{A}^{III-} \\ \vec{A}^{II2-} \\ \vec{A}^{II3-} \\ \vec{A}^{II4-} \end{pmatrix}. \tag{6}$$

At the step discontinuities at $z = t$ (end of the screen with finite length $t$, Fig. 2(a)), the following relations hold, analogously to (5):

$$\vec{B}^{III-} + \vec{B}^{III+} = \sum_{\eta=1}^{4} (L^{(\eta)}) \cdot [\vec{B}^{II(\eta)-} + \vec{B}^{II(\eta)+}]$$

$$(N^{(\eta)}) \cdot [B^{III-} - B^{III+}] = B^{II(\eta)-} - B^{II(\eta)+} \tag{7}$$

where $\eta = 1,2,3,4$. Equation (7) leads to the scattering matrix at $z = t$

$$\begin{pmatrix} \vec{B}^{III+} \\ \vec{B}^{III-} \\ \vec{B}^{II2-} \\ \vec{B}^{II3-} \\ \vec{B}^{II4-} \end{pmatrix} = (S)_{z=t} \begin{pmatrix} \vec{B}^{III-} \\ \vec{B}^{III+} \\ \vec{B}^{II2+} \\ \vec{B}^{II3+} \\ \vec{B}^{II4+} \end{pmatrix}. \tag{8}$$

For the calculation of the scattering matrix of the total screen structure (Fig. 2(a))

$$\begin{pmatrix} \vec{A}^{I-} \\ \vec{B}^{III+} \end{pmatrix} = \begin{pmatrix} (S_{11}) & (S_{12}) \\ (S_{21}) & (S_{22}) \end{pmatrix}_{screen} \cdot \begin{pmatrix} \vec{A}^{I+} \\ \vec{B}^{III-} \end{pmatrix} \tag{9}$$

the relations between the wave amplitudes along the $\eta$ corresponding intermediate waveguide sections have to be taken into account

$$\vec{A}^{II(\eta)-} = (R^{(\eta)})\, \vec{B}^{II(\eta)-}$$

$$\vec{B}^{II(\eta)+} = (R^{(\eta)})\, \vec{A}^{II(\eta)+} \tag{10}$$

where $(R^{(\eta)})$ is the diagonal matrix

$$(R^{(\eta)}) = \begin{pmatrix} e^{-jk_{z1}^{II(\eta)} \cdot t} & & & 0 \\ & e^{-jk_{z2}^{II(\eta)} \cdot t} & & \\ & & \ddots & \\ 0 & & & e^{-jk_{zm}^{II(\eta)} \cdot t} \end{pmatrix}. \tag{11}$$

The corresponding relations which lead to the scattering matrix elements in (9) are given in the Appendix. Opposite to the common treatment with transmission matrices, this direct combination of scattering matrix elements leads to expressions containing exponential functions with only negative argument (cf. (11)). So the hitherto known numerical instabilities due to resonance and interference effects of higher order modes below their cutoff frequencies may be avoided.

The series connection of screens may be treated in a similar manner. The scattering matrix, e.g., for two screens (Fig. 2(b)), is given by

$$\begin{pmatrix} \vec{A}^- \\ \vec{D}^+ \end{pmatrix} = \begin{pmatrix} (S_{11}) & (S_{12}) \\ (S_{21}) & (S_{22}) \end{pmatrix}_{two\ screens} \cdot \begin{pmatrix} \vec{A}^+ \\ \vec{D}^- \end{pmatrix} \tag{12}$$

the elements of which are composed (cf. Appendix) of the two scattering matrix elements of the screens (cf. (9)) and the diagonal matrix $(R)_{wg}$ of the intermediate waveguide section with the length $l$

$$(R)_{wg} = \begin{pmatrix} e^{-jk_{z1}^{(I)} \cdot l} & & 0 \\ & \ddots & \\ 0 & & e^{-jk_{zm}^{(I)} \cdot l} \end{pmatrix} \tag{13}$$

with $k_{zm}^{(I)} = \omega^2 \mu\epsilon - (m\pi/a)^2$ (cf. (3)).

The overall matrix for more than two screens is found analogously.

For the calculations in this paper, the expansion into twenty eigenmodes at each discontinuity yields sufficient convergence behavior of the scattering matrix coefficients.

## III. Results

First, a small-band one-resonator filter example is investigated for which also a round post filter curve (including higher order mode interaction) is available in a limited frequency range [8]. Fig. 3 compares the insertion-loss behavior of this filter-type using several inductive obstacle structures as reactance elements with nearly identical susceptances, but different physical geometry: round post [8], quadratic post, broadside oriented strip, triplet of quadratic posts, iris-coupled structures, and triplet of broadside oriented strips. Fig. 3(a) shows the agreement of the filter curve between the round post filter [8] (small circles) and the quadratic post structure (solid line), calculated with the field expansion method for single metal inserts [2]; the length $c$ of the side of the quadratic post is given by the circular to rectangular cross-section equivalence relations of inductive posts [13].

This equivalent quadratic structure is used in Fig. 3(b) to simulate the round post filter for a broader frequency range (30–55 GHz) in order to investigate the stopband attenuation behavior. From Fig. 3(b), it may be stated that the broadside-oriented strip structure (solid line) achieves better stopband attenuation than the quadratic post structure (dashed line); the broadside dimension $w$ of the strip (with given thickness $t = 0.19$ mm) is determined also by the equivalence relations of [13] and slightly corrected to yield nearly identical 3-dB bandwidth of the filters in order to enable a fair comparison of the filter behavior.

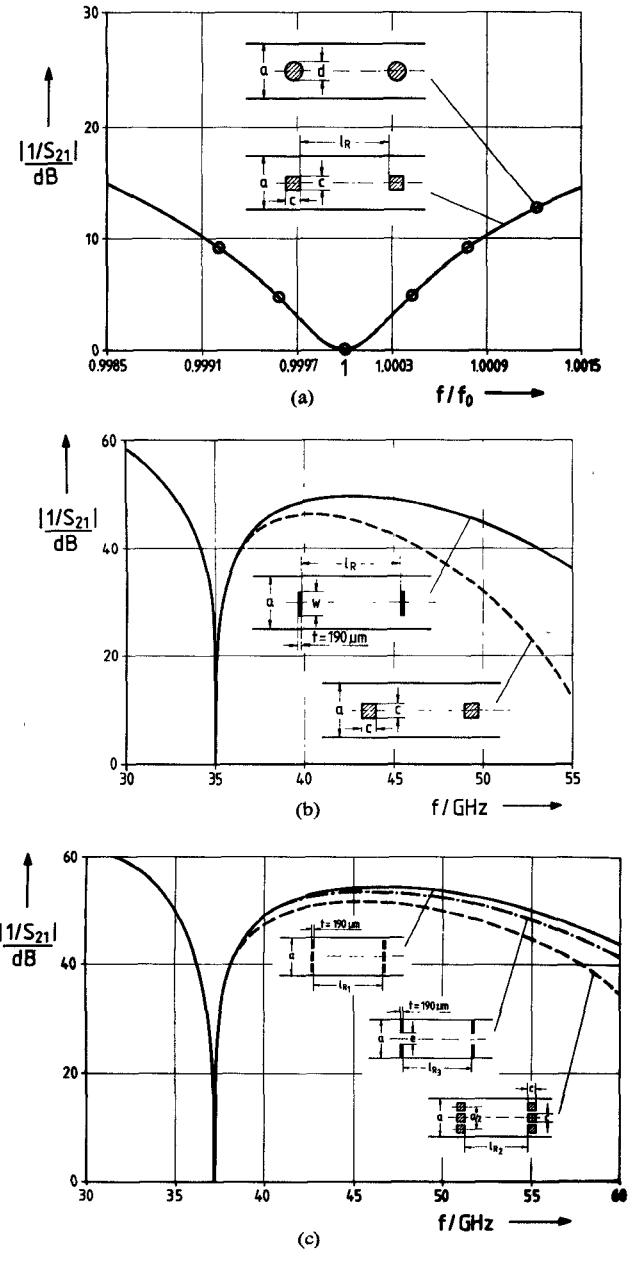


Fig. 3. Insertion loss $|1/S_{21}|$ in decibels as a function of frequency for small-band inductive obstacle coupled one-resonator filters with reactance elements of different physical geometry but nearly identical susceptance; 3-dB bandwidth $\Delta f/f_0 \approx 0.06$ percent; waveguide housing dimensions $a = 7.112$ mm, $b = 3.556$ mm (*Ka*-band). (a) Quadratic posts $c = 1.804$ mm $= 2d/2.365$ [13], $l_R = 4.866$ mm, calculated with the orthogonal expansion method, cf. [2]; ○○○ round posts, results of [8], $d/a = 0.3$ [8]. (b) —— broadside-oriented strips $w = 3.390$ mm, $t = 0.19$ mm, $l_R = 5.210$ mm, solid line; ---- quadratic posts (dimensions cf. (a)), dashed line; calculated with the orthogonal expansion method, cf. [2]. (c) —— triplet of broadside-oriented strips, $t = 0.19$ mm, $p_1 = 0.84$ mm, $m_2 = 2.09$ mm, $p_2 = 2.93$ mm, $m_3 = 4.18$ mm, $p_3 = 5.02$ mm, $m_4 = 6.27$ mm, (cf. Fig. 1(b)), $l_{R_1} = 4.81$ mm, solid line; ---- triplet of quadratic posts $c = 0.665$ mm, $l_{R_2} = 4.62$ mm, dashed line. - - - - inductive iris-coupled filter $e = 1.004$ mm, $l_{R3} = 4.785$ mm, dashed–dotted line.

Fig. 3(c) shows the insertion loss versus frequency of the corresponding filters with a triplet of broadside-oriented strips (solid line) and with a triplet of quadratic posts (dashed line); the strips and posts dimensions again are determined so to achieve nearly identical 3-dB bandwidth, and the midband frequency is chosen ($f_0 \approx 37$ GHz) to be near at the band end (40 GHz) of the *Ka*-band waveguide because the influence of the higher order mode interactions is more severe beyond the band end than within the fundamental mode waveguide band (26–40 GHz). For further comparison, an iris-coupled one-resonator filter curve (dashed–dotted line) is included, which is calculated by the field expansion in the eigenmodes method described in [14]. Again, it can be stated that the broadside-oriented strips achieve slightly better stopband attenuation behavior than the quadratic post and the iris-coupled structure. A possible explanation may be the increased cutoff frequencies of the higher order modes within the reactance element section, which is achieved by the smaller interstices of the broadside-oriented strip structure in comparison with quadratic (or round) posts and irises of nearly identical susceptance. For a complete discussion of these effects, the $Q$-factor properties of the related resonator structures should also be taken into account, which would go, however, beyond the limits of this paper, since effects of losses are not included in the analysis given.

For the design of the two-resonator screen filters of Table I, an error function $F(\bar{x})$ to be minimized is defined [12]

$$F(\bar{x}) = \sum_{i=1}^{N_s} \left(a_{s\min}/a_{21}(f_i)\right)^2 + \sum_{i=1}^{N_p} \left(a_{21}(f_i)/a_{p\max}\right)^2 \stackrel{!}{=} \text{Min} \tag{14}$$

where $N_s$ and $N_p$ are the number of frequency sample points $f_i$ in the stopband and passband, respectively, $a_{s\min}$ and $a_{p\max}$ are the given minimum stopband and maximum passband attenuation levels, respectively, and $a_{21} = 20\log(1/|S_{21}|)$ is the calculated overall filter insertion loss. For given waveguide housing dimensions, thickness $t$ of the metallic inserts, the parameters to be optimized are the screen dimensions (Table I). The resonator lengths $l_R$ for these designs are chosen to yield midband frequencies in the near of the higher *Ku*-band (12.6–18 GHz) and higher *Ka*-band (26–40 GHz) ends, respectively. Compared with the lumped-element circuit-type approach for filter designs [6], this computer optimization takes into account higher order mode coupling effects and, therefore, achieves correct design data.

Fig. 4 shows the calculated insertion loss of a two-resonator *Ka*-band (cf. Table I) *E*-plane screen filter (solid line) in comparison with a planar circuit single-metal-insert filter [2], also with two resonators and with a 3-dB bandwidth of about 0.5 percent. The peak attenuation in the second stopband for the triple-insert screen filter is 70 dB, whereas the single-insert filter achieves only about 34 dB. The triple quadratic post filter, for comparison, shows about 63-dB peak attenuation (dashed–dotted line).

The calculated and measured insertion loss of a *Ku*-band screen filter (Table I) is shown in Fig. 5. The theoretical minimum insertion loss of 0.2 dB in Table I is principally reflection loss. The measured value is 0.8 dB. The maximum tolerances of the metal-etched screen dimensions in relation to the optimized data are about $\pm 50$ $\mu$m, which has been checked by a microscope for the fabricated *Ku*-band prototype (Fig. 6.). The material of the screens is 99.0-percent pure copper. The screens are fixed in the waveguide housing by alignment pins.

## IV. Conclusion

*E*-plane integrated screen filters using triple-strip elements to suppress higher order modes achieve filter designs with high peak attenuation in the upper stopband, and also for midband frequencies in the near of the higher band end of the waveguide housing. The design is based on a rigorous field expansion into incident and scattered waves at all discontinuities. This allows direct inclusion of both higher order mode coupling and finite

TABLE I
COMPUTER-OPTIMIZED DESIGN DATA FOR TWO-RESONATOR *E*-PLANE SCREEN FILTERS

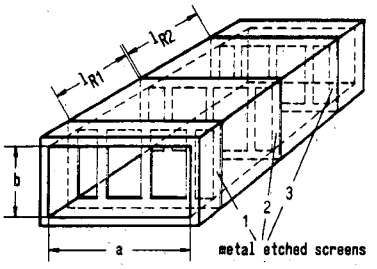


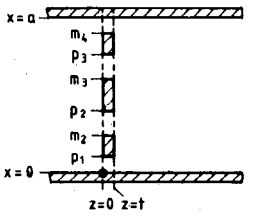


( Screen material: 99.9 % pure copper )

| Frequency-band for the filter design waveguide housing | Screen thickness t ( mm ) | Resonator length $l_R$ ( mm ) | Screen number | $p_1$ ( mm ) | $m_2$ ( mm ) | $p_2$ ( mm ) | $m_3$ ( mm ) | $p_3$ ( mm ) | $m_4$ ( mm ) | Midband-frequency ( GHz ) | 3 dB-band-width ( MHz ) | min.passband insertion-loss ( dB ) | Remarks |
|---|---|---|---|---|---|---|---|---|---|---|---|---|---|
| Ku - band a = 15.798 mm b = 7.88 mm | 0.19 | $l_{R1} = l_{R2}$ 10.000 | 1 | 3.350 | 4.550 | 7.299 | 8.499 | 11.248 | 12.448 | 17.08 | 200 | 0.2 | Theory |
| | | | 2 | 2.600 | 5.300 | 6.549 | 9.249 | 10.498 | 13.198 | | | | |
| | | | 3 | 3.350 | 4.550 | 7.299 | 8.499 | 11.248 | 12.448 | | | | |
| | | | 1 | 3.347 | 4.559 | 7.305 | 8.520 | 11.255 | 12.493 | 17.132 | 220 | 0.8 | Measured |
| | | | 2 | 2.600 | 5.300 | 6.565 | 9.262 | 10.497 | 13.210 | | | | |
| | | | 3 | 3.345 | 4.563 | 7.310 | 8.533 | 11.258 | 12.505 | | | | |
| Ka - band a = 7.112 mm b = 3.556 mm | 0.19 | $l_{R1} = l_{R2}$ 4.500 | 1 | 1.503 | 2.053 | 3.281 | 3.831 | 5.059 | 5.609 | 38.16 | 180 | 0 | Theory |
| | | | 2 | 1.128 | 2.428 | 2.906 | 4.206 | 4.684 | 5.984 | | | | |
| | | | 3 | 1.503 | 2.053 | 3.281 | 3.831 | 5.059 | 5.609 | | | | |

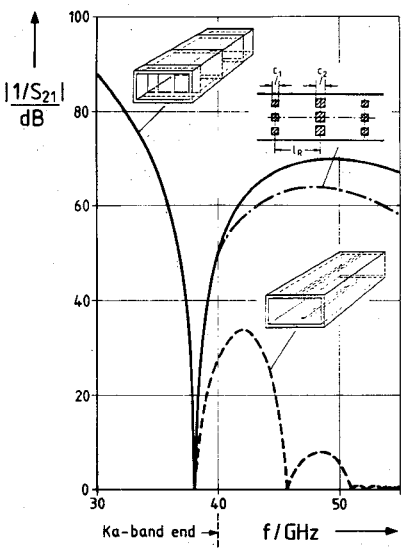


Fig. 4. Insertion loss $|1/S_{21}|$ in decibels as a function of frequency for *Ka*-band two-resonator filters with about 0.5-percent 3-dB bandwidth. —— triple-strip screen filter (dimensions cf. Table I). ---- planar circuit single-metal-insert filter (calculated according to [2]). - - - - - triple quadratic post filter (*Ka*-band waveguide) $l_R = 4.300$ mm, $c_1 = 0.35$ mm, $c_2 = 0.81$ mm.

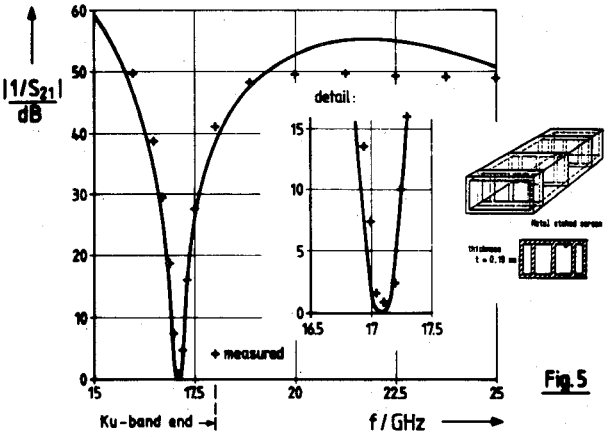


Fig. 5. Calculated and measured insertion loss $|1/S_{21}|$ in decibels as a function of frequency for a *Ku*-band two-resonator triple-strip screen filter (cf. Table I) with about 1.2-percent 3-dB bandwidth. (The measuring limit of the test assembly was 50 dB.)

strip thickness. An optimizing computer program leads to *Ku*-band and *Ka*-band screen filters which may be fabricated by the metal-etching technique. This is appropriate for mass-production and avoids the necessity for tuning devices. Since the finite metal thickness and the higher order mode interaction is included in the design, measurements show good coincidence with theoretical predicted values. This is demonstrated at a two resonator *Ku*-band waveguide screen filter, which yields 0.8-dB measured minimum passband insertion loss. Calculated insertion loss up to 70 GHz

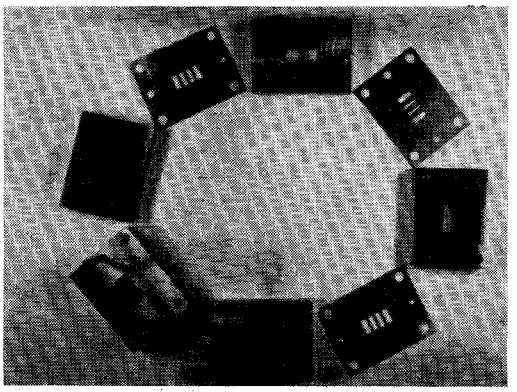

Fig. 6. Photograph of the opened *Ku*-band waveguide two-resonator screen filter (metal-etched screens and waveguide sections).

for a *Ka*-band prototype in the upper stopband shows the good stopband attenuation behavior of this class of *E*-plane integrated waveguide screen filters.

## Appendix

### A. Matrix Elements $(L^{(\eta)})$, $(N^{(\eta)})$ in (4)

$$L_{ij}^{(1)} = H_{ij}^{(1)} \cdot \frac{2}{\sqrt{p_1 \cdot a}} \sqrt{\frac{k_{zi}^{(\mathrm{I})}}{k_{zj}^{(\mathrm{III})}}}$$

$$H_{ij}^{(1)} = \int_0^{p_1} \sin\frac{i\pi}{a}x \sin\frac{j\pi}{p_1}x\,dx \tag{A1}$$

$$L_{ij}^{(2)} = H_{ij}^{(2)} \cdot \frac{2}{\sqrt{a(p_2 - m_2)}} \cdot \sqrt{\frac{k_{zi}^{(\mathrm{I})}}{k_{zj}^{(\mathrm{II2})}}}$$

$$H_{ij}^{(2)} = \int_{m_2}^{p_2} \sin\frac{i\pi}{a}x \sin\frac{j\pi}{p_2 - m_2}(p_2 - x)\,dx \tag{A2}$$

$$L_{ij}^{(3)} = H_{ij}^{(3)} \cdot \frac{2}{\sqrt{a(p_3 - m_3)}} \cdot \sqrt{\frac{k_{zi}^{(\mathrm{I})}}{k_{zj}^{(\mathrm{II3})}}}$$

$$H_{ij}^{(3)} = \int_{m_3}^{p_3} \sin\frac{i\pi}{a}x \sin\frac{j\pi}{p_3 - m_3}(p_3 - x)\,dx \tag{A3}$$

$$L_{ij}^{(4)} = H_{ij}^{(4)} \cdot \frac{2}{\sqrt{a(a - m_4)}} \cdot \sqrt{\frac{k_{zi}^{(\mathrm{I})}}{k_{zj}^{(\mathrm{II4})}}}$$

$$H_{ij}^{(4)} = \int_{m_4}^{a} \sin\frac{i\pi}{a}x \sin\frac{j\pi}{a - m_4}(a - x)\,dx. \tag{A4}$$

$(N^{(\eta)})$ is the transposed matrix $(L^{(\eta)})'$ and $k_{zm}^{(\nu)}$ is the wavenumber (cf. (3)).

### B. Scattering Matrix Elements in (9)

$$(S_{11})_{\text{screen}} = -\left[(E)+(P)-(Q)\cdot((E)+(P))^{-1}\cdot(Q)\right]^{-1} \cdot\left[(E)-(P)+(Q)\cdot((E)+(P))^{-1}\cdot(Q)\right] \tag{A5}$$

$$(S_{12})_{\text{screen}} = -\left[(E)+(P)-(Q)\cdot((E)+(P))^{-1}\cdot(Q)\right]^{-1} \cdot\left[(Q)+(Q)\cdot((E)+(P))^{-1}\cdot((E)-(P))\right] \tag{A6}$$

$$(S_{21})_{\text{screen}} = -\left[(E)+(P)-(Q)\cdot((E)+(P))^{-1}\cdot(Q)\right]^{-1} \cdot\left[(Q)+(Q)\cdot((E)+(P))^{-1}\cdot((E)-(P))\right. \tag{A7}$$

$$(S_{22})_{\text{screen}} = -\left[(E)+(P)-(Q)\cdot((E)+(P))^{-1}\cdot(Q)\right]^{-1} \cdot\left[(E)-(P)+(Q)\cdot((E)+(P))^{-1}\cdot(Q)\right] \tag{A8}$$

where

$$(P) = \sum_{\eta=1}^{4} (L^{(\eta)})\cdot\left[(E)-2\cdot\left((R^{(\eta)})-(R^{(\eta)})^{-1}\right)^{-1}\cdot(R^{(\eta)})\right] \cdot(N^{(\eta)}) \tag{A9}$$

$$(Q) = \sum_{\eta=1}^{4} (L^{(\eta)})\cdot\left[2\cdot\left((R^{(\eta)})-(R^{(\eta)})^{-1}\right)^{-1}\right]\cdot(N^{(\eta)}) \tag{A10}$$

$(E)$ = unity matrix
$(R)$ cf. (11).

### C. Scattering Matrix Elements in (12)

$$(S_{11})_{\text{two screens}} = (S_{11}^{(1)}) + (S_{12}^{(1)})\cdot(R)_{wg} \cdot\left[(E)-(S_{11}^{(2)})\cdot(R)_{wg}\cdot(S_{22}^{(1)})\cdot(R)_{wg}\right]^{-1} \cdot(S_{11}^{(2)})\cdot(R)_{wg}\cdot(S_{21}^{(1)}) \tag{A11}$$

$$(S_{12})_{\text{two screens}} = (S_{12}^{(1)})\cdot(R)_{wg} \cdot\left[(E)-(S_{11}^{(2)})\cdot(R)_{wg}\cdot(S_{22}^{(1)})\cdot(R)_{wg}\right]^{-1}\cdot(S_{12}^{(2)}) \tag{A12}$$

$$(S_{21})_{\text{two screens}} = (S_{21}^{(2)})\cdot(R)_{wg}\cdot\left[(E)-(S_{22}^{(1)})\cdot(R)_{wg} \cdot(S_{11}^{(2)})\cdot(R)_{wg}\right]^{-1}\cdot(S_{21}^{(1)}) \tag{A13}$$

$$(S_{22})_{\text{two screens}} = (S_{22}^{(2)}) + (S_{21}^{(2)})\cdot(R)_{wg} \cdot\left[(E)-(S_{22}^{(1)})\cdot(R)_{wg}\cdot(S_{11}^{(2)})\cdot(R)_{wg}\right]^{-1} \cdot(S_{22}^{(1)})\cdot(R)_{wg}\cdot(S_{12}^{(2)}) \tag{A14}$$

where

$(E)$ = unity matrix
$(R)_{wg}$ cf. (13).

## References


[1] Y. Konishi and K. Uenakada, "The design of a bandpass filter with inductive strip—Planar circuit mounted in waveguide," *IEEE Trans. Microwave Theory Tech.*, vol. MTT-22, pp. 869–873, Oct. 1974.

[2] R. Vahldieck, J. Bornemann, F. Arndt, and D. Grauerholz, "Optimized waveguide *E*-plane metal insert filters for millimeter-wave applications," *IEEE Trans. Microwave Theory Tech.*, vol. MTT-31, pp. 65–69, Jan. 1983.

[3] J. Bornemann, F. Arndt, R. Vahldieck, and D. Grauerholz, "Double planar integrated millimeter-wave filter," in *Proc. 13th European Microwave Conf.*, (Nürnberg), 1983, pp. 168–173.

[4] G. Graven and L. Lewin, "Design of microwave filters with quarter-wave couplings," *Proc. Inst. Elec. Eng.*, vol. 103B, pp. 173–175, Mar. 1956.

[5] L. Lewin, *Theory of Waveguides*. New York: Wiley, 1975.

[6] G. L. Matthaei, L. Young, and E. M. T. Jones, *Microwave Filters, Impedance Matching Networks, and Coupling Structures*. New York: McGraw-Hill, 1964.

[7] E. A. Mariani, "Designing narrow-band triple-post waveguide filters," *Microwaves*, vol. 4, pp. 93–97, 1965.

[8] P. G. Li, A. T. Adams, Y. Leviatan, and J. Perini, "Multiple-post inductive obstacles in rectangular waveguides," *IEEE Trans. Microwave Theory Tech.*, vol. MTT-32, pp. 365–373, Apr. 1984.

[9] H. Auda and R. F. Harrington, "Inductive posts and diaphragms of arbitrary shape and number in a rectangular waveguide," *IEEE Trans. Microwave Theory Tech.*, vol. MTT-32, pp. 606–613, June 1984.

[10] K. Chang and P. J. Khan, "Analysis of three narrow transverse strips in waveguide," in *1978 IEEE S-MTT Inst. Microwave Symp. Dig.*, pp. 419–421.

[11] K. Chang, "Impedance calculation of three resonant strips on the transverse plane of a rectangular waveguide," *IEEE Trans. Microwave Theory Tech.*, vol. MTT-32, pp. 126–130, Jan. 1984.

[12] H. Schmiedel, "Anwendung der Evolutionsoptimierung auf Schaltungen der Nachrichtentechnik," *Frequenz*, vol. 35, pp. 306–310, Nov. 1981.

[13] N. Marcuvitz, *Waveguide Handbook*. New York: McGraw-Hill, 1951, ch. 5.11.

[14] H. Patzelt and F. Arndt, "Double-plane steps in rectangular waveguides and their application for transformers, irises, and filters," *IEEE Trans. Microwave Theory Tech.*, vol. MTT-30, pp. 771–776, May 1982.